Effect of propylene glycol ether fuelling on the different physico-chemical properties of the emitted particulate matters:

Tsolakis, Athanasios; Serhan, Nahil; Martos, F. J.

DOI:
10.1016/j.fuel.2018.01.065

Effect of propylene glycol ether fuelling on the different physico-chemical properties of the emitted particulate Matters: implications of the soot reactivity

N. Serhan[a], A. Tsolakis[a], F.J. Martos[b]

[a] Mechanical Engineering, University of Birmingham, Birmingham B15 2TT, UK
[b] Escuela de Ingenierías Industriales, University of Málaga, 29071 Málaga, Spain

Abstract

The research work presented here focuses on the particulate matter (PM) number concentration and its physico-chemical properties from the combustion of di and tri-propylene glycol methyl ether/diesel blends (D20 and T20 respectively). Exhaust PM were characterised using a Scanning Transmission electron microscopy equipped with energy dispersive X-ray spectroscopy (S/TEM-EDX) to quantify the nanostructure, morphology and elemental composition of the agglomerates, Raman spectroscopy (RS) to further examine the particulate graphite like structure and thermo-gravimetric analyser (TGA) to analyse the oxidative reactivity. The increase in the fuel oxygen content reduces both, exhaust PM levels and NOx emissions. TGA analysis confirms that the oxygenated blends enhance the particulates oxidative reactivity and increase their volatile fraction in the following order T20>D20>Diesel. EDX analysis shows that the combustion of both D20 and T20 lowers the PM carbon fraction and ash precipitations but increases its oxygen functional groups in the same order. Furthermore, a notable reduction in the primary particles size was recorded, whose carbon layers were found to be more tortuous than diesel, but no significant modification was shown in their length. Unconventionally, smaller separation distance was seen between the carbon layers, and higher graphitisation order was seen from the RS analysis. It was finally concluded that concerning the nanoscale parameters, the initial curvature of the carbon layers present a stronger influence in dictating the particles reactivity compared to the graphitisation order or the initial length and separation distance of the carbon layers. As for the macroscale, primary particle size and the portion of oxygen in the particle could be another possible reason for the better soot reactivity seen from the propylene glycol ethers combustion. The significance of the reduced exhaust particles' level and modified PM's physical and elemental properties can improve Diesel Particulate Filter (DPF) regeneration and allows engine calibration that can favour NOx emissions reduction (i.e. lower NOx – PM trade-off lines).

Keywords: Glycol ethers; Raman spectrometry; Soot reactivity; Thermogravimetric; nanostructure; elemental analysis; emissions; tortuosity

1. Introduction

Particulate Matter (PM) emissions from modern vehicles, including diesel and gasoline direct injection (GDI), consist of carbonaceous materials (soot) and various types of inorganic and organic substances, some being mutagenic and carcinogenic by nature [1]. It is commonly accepted that oxygen-borne fuels blended with diesel can effectively reduce the PM levels and other unregulated emissions such as unburned hydrocarbons and carbon oxides [2]. They also play an important role in enhancing the oxidation reactivity of the soot particles (ability to oxidise) [3], leading to improved particulate filters function and durability by lowering the regeneration temperatures and minimising the intensity of the soot burn-off cycles [3].

If the biodiesel production and utilisation is increased to cover the energy demand in transportation, then the associated increase of the glycerol volumes (main by-product from biodiesel production) may create ecological hazards, since they cannot be safely disposed [4]. One possible application to benefit from these products could be to synthesise propylene oxides from the resulted glycerol, following the process described by Yu et al [5]. Afterwards, propylene glycol ethers could be produced by the reaction of propylene oxides with methanol [6]. Similar to biodiesel, glycol ethers are known for their suitability with compression ignition engines in terms of safety, accessibility, price and compatibility with diesel fuel [7]. Their atomic structure contains both ether and alcohol moieties and generally characterised with a high oxygen content [8].

Tri-propylene glycol methyl ether (TPGME) was nominated by Natarajan et al. [9] and also suggested by Gonzalez et al. [2] as a potential oxygenate to be blended with diesel among 71 candidates, taking into account several factors such as exhaust emissions reduction, blend toxicity, lubricity and cetane number improvement. Following Gonzalez's work, both Mueller et al. [10] and Burke et al. [6] incorporate numerical simulations along with chemical kinetic modeling to examine the effect of TPGME molecular structure on the ignition mechanism and the soot formation process. As a result, TPGME was shown to effectively reduce the soot precursors inception, especially acetylene, and that was directly linked to its optimal atomic structure where all the oxygen atoms are available for soot reduction. Dumitrescu et al. [11] studied the ignition delay and flame lift-off length produced by TPGME/Diesel blend (50% vol.) and confirmed a reduction in soot formation and/or increase in soot oxidation. Another glycol ether candidate is the di-propylene glycol methyl ether (DPGME), with similar chemical structure as TPGME but present shorter carbon chain length and one less oxygen atom, resulting in approximately the same oxygen content. Natarajan et al. [9] nominates DPGME as a viable candidate for mixing with diesel in terms of PM reduction and blend stability. Gomez-Cuenca et al. [8] reported that DPGME/diesel fuel blends enhanced the mixture cetane number and reduced CO, while no clear trend was seen in production of THC, NOx and PM emissions. Hilden et al. [12] reported that both DPGME and TPGME diesel blends, with 6.5 wt.% oxygen content, present comparable PM reduction capability, while other authors [9] found that under the same oxygen content of 7 wt.%, TPGME/diesel blends are more efficient in reducing PM emissions than DPGME blends.

Although propylene glycol ethers are proved to be suitable for mixing with diesel and can reduce the PM discharges, there's still no study highlighting their effect on the resulted PM characteristics. The PM physical and chemical properties, such as primary particle size, carbon layer structure, oxygen functional groups and

the corresponding ash content are reported to guide the particles reactivity [13]. Despite the extensive analysis conducted to understand the correlation between these variables and the oxidative behaviour of the particles, this relationship is still quite complex and not fully understood in the literature [13-15]. The current paper aims to obtain an improved understanding of the level at which DPGME and TPGME diesel blends (20% vol.) will influence the PM oxidative reactivity, and determine the effect of the different physico-chemical properties, such as morphological parameters, nanostructure characteristics and elemental composition, on the corresponding reactivity.

2. Experimental set up and methodology

2.1: Engine test and combustion analysis:

The experiments have been conducted in a four-stroke research diesel engine featured with a common rail fuel injection system that permits the control of multiple injection strategies. The main specifications of the test engine can be found in Table 1. All the tests were performed at a constant speed of 1500 rpm and fix load of 4 bar IMEP. The fuel was injected at a stable pressure of 600 bars and split between pilot and main-injections, with timings of 15 and 8 CAD BTDC respectively. In-cylinder pressure was recorded over 200 cycles using an AVL GH13P pressure sensor mounted in the cylinder head and the signal was amplified by an AVL FlexiFEM 2P2 Amplifier. The corresponding Digital shaft encoder producing 360 pulses per revolution was used to measure the crank shaft position [16]. Heat release rate (HRR) was integrated from the pressure data collected by designing a simple model neglecting the heat losses differences between the fuels tested. Exhaust temperatures from the combustion of each fuel blend are recorded with the use of K-type thermocouples (with a range of 0-1250 ^{o}C and an accuracy of ± 2.2 °C) located directly at the exhaust port.

Table 1: Diesel engine specifications

Engine Parameters	Specifications
Engine type	Diesel 1-cylinder
Stroke type	Four-stroke
Cylinder bore x stroke (mm)	84 x 90
Connecting rod length (mm)	160
Compression ratio	16:01
Displacement (cc)	499
Engine speed range (rpm)	900-3000
IMEP range (bar)	<7
Fuel pressure range (bar)	500-2000
Number of injections	3 injection events

2.2 Fuel used:

Ultra-low sulphur diesel (ULSD) was supplied from Shell Global Solutions UK, DPGME and TPGME were purchased from Sigma Aldrich. Glycol ether diesel blends, so called D20 and T20 in this analysis, were

prepared by mixing diesel with each of the candidates (DPGME and TPGME respectively) separately to form 6.5% wt. oxygen content. The properties of the oxygenated hydrocarbons and the blends are obtained from the literature and presented in Table 2.

Table 2: Fuel specification [12]

	Test method	**ULSD**	**DPGME**	**TPGME**	**D20[a]**	**T20**
Chemical Formula	**-**	$C_{14}H_{26.1}$	$C_7H_{16}O_3$	$C_{10}H_{22}O_4$	-	-
Latent Heat of vaporisation (kJ/kg)	**-**	243	330 [17]	357 [18]	-	-
FAME % (v/v)	**EN14078-A**	<0.05	-	-	<0.05	<0.05
Viscosity (cSt T 40 c)	**D-445**	2.395	-	-	2.208	2.359
Lubricity, SLBOCLE, g	**D-5001**	3700	-	-	2900	4100
Density (kg/m^3) at 20 ^{o}C	**D-1298**	826.9	938 [9]	968 [9]	846.1	848.8
Cetane number	**D-6890**	43.4 [19]	43.9 [20]	80 [6]	-	-
LCV (MJ/kg)	**D-3338**	43.11	27.5 [17]	28.1 [21]	39.58	39.55
Sulphur, ppm mass	**D-3120**	<5	-	-	<5	<5
Cloud point	**D-2500**	-21			-20	-20
Flash point	**D-93**	71	74 [9]	>110 [9]	72	76
Ash, mass %	**D-482**	<0.01	-	-	<0.01	<0.01
10 % distillation (^{o}C)	**D-86**	208.6	-	-	191.8	207.8
50% distillation (^{o}C)	**D-86**	260.3	-	-	251.5	244.8
90 % distillation (boiling temperature) (^{o}C)	**D-86**	319.2	-		313.5	308.5
wt.% C	**Calculated**	86.47	56.73	58.22	80.5	80.55
wt.% H	**Calculated**	13.53	10.88	10.75	13	12.95
wt.% O	**Calculated**	0	32.39	31.03	6.5	6.5
Oxygenates vol. (%)	**Calculated**	-	-	-	20.07	20.95

[a] The properties presented for D20 corresponds for 6.1 wt.% oxygen content blend (no information for the 6.5% wt.% O was available in the literature)

2.3: Gaseous Emissions analysis and Particle number concentration:

Multi-Gas 2030 FTIR spectrometry-based analyser was utilised to measure the gaseous emission from the exhaust such as nitrogen oxides (NOx), carbon oxides (CO-CO_2) and total hydrocarbons (THC).

Electrical mobility particle size distribution (dp) and the total particle number concentration were measured using a TSI scanning mobility particle sizer which includes a 3080-electrostatic classifier, 3081-Differential Mobility Analyser and a 3775-Condensation Particle Counter [22]. The exhaust dilution ratio was set to 1:11 using an ejector diluter system before testing the sample.

2.4: PM collection method

Tissue quartz (TQ) filters (type TISSUEQTZ 2500 QAT-up, 47mm diameter) supplied from VWR International Ltd UK were applied to collect the needed PM samples. The filters were pre-heated at 650^{o}C for 3 hours before starting the collection process. Afterwards, they were placed in an inline filter holder connected to a partial exhaust line (vacuum-pumped assisted, as shown in Figure 1) and loaded to a target mass of 3 mg, following the method proposed by Mühlbauer et al. [13]. The samples collection point was placed before the Diesel Oxidation Catalyst (DOC) to maintain the particles volatile fraction and prevent any possible low-temperature PM oxidation that may be caused by the increased amounts of NO_2 produced downstream the catalyst. This type of reactions may alter the particles structural order and affect their oxidative reactivity [23].

2.5: PM characterisation techniques:

A schematic diagram presenting the production process of the tested oxygenated hydrocarbons (from literature) and the experimental procedure used for the soot collection and the different methods used to analyse the particles physico-chemical properties is plotted in figure 1.

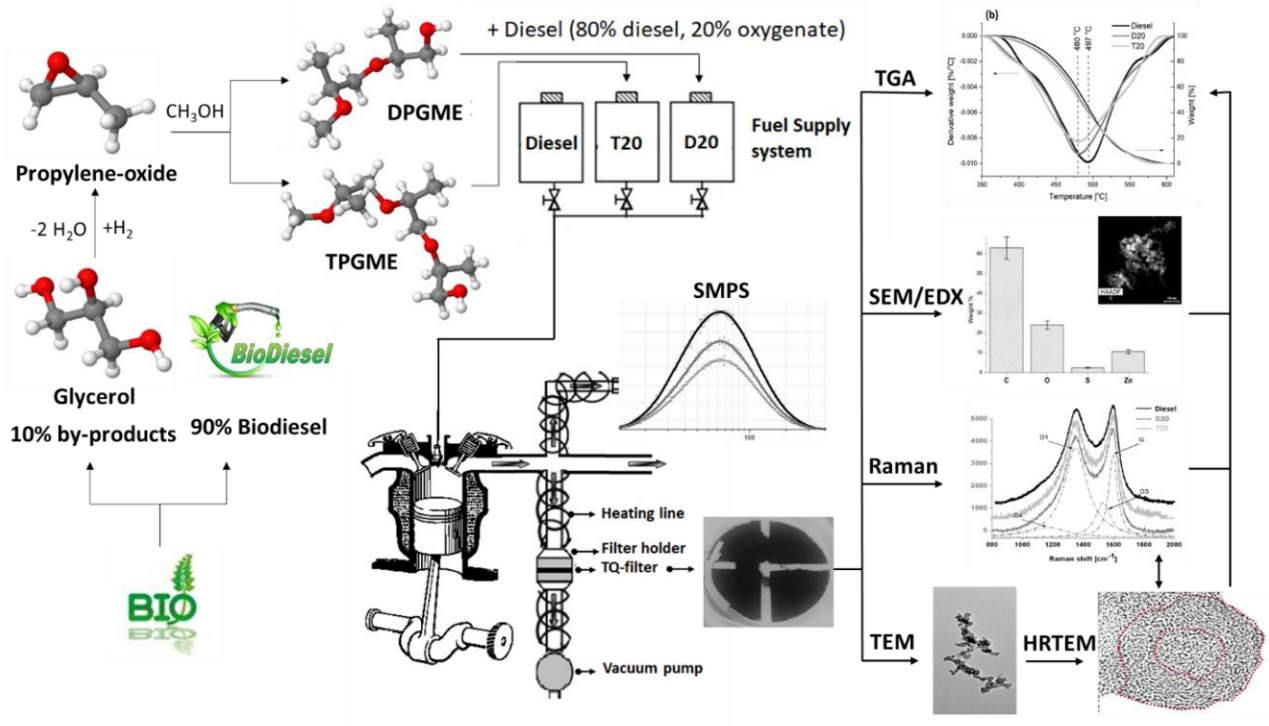

Figure 1: Schematic diagram of the fuel origin, experimental facility, sampling techniques and testing methods

2.5.1: TGA analysis

The TQ-filters were cut into small sections and used for the TGA testing (PerkinElmer) in a way that an equal PM mass of ~ 0.12 mg was examined in all the experiments [24]. The sample was first heated under an inert atmosphere of nitrogen at a constant flow of 40 ml/min with 10 °C/min ramp to reach 400 °C. The PM sample was maintained isothermal for 30 min to ensure that all the volatile fraction is evaporated, then

cooled down to 200°C to start the carbon oxidation process. Atmosphere was then changed to air (10% O_2, 90% N_2) and the PM sample was heated to 650 °C with a ramp of 3 °C/min under a flow of 40 ml/min. The PM thermal behaviour was identified following two different methods: (a) The 1st derivative of the percentage weight loss (dm/dt) was calculated to determine the soot ignition temperature (explained in detail in section 3.3.1) [13, 25], and (b) Soot activation energy (Ea) was determined following the simplified Arrhenius-type reaction model:

$$\ln\left(-\frac{1}{m}\frac{dm}{dt}\right) = \frac{-E_a}{R}\left(\frac{1}{T}\right) + ln(A_{P_{O_2}}) \qquad \text{(eq.1)}$$

where m is the percentage sample mass (%), R the universal gas constant (8.314 J/mol.K), T temperature (in Kelvin), and P_{O2} oxygen partial pressure. The soot activation energy was obtained from the slope of the plot of $\ln\left(-\frac{1}{m}\frac{dm}{dt}\right)$ vs. $\frac{1}{T}$ [3].

2.5.2: EDX analysis:

FEI Talos™ F200X S/TEM equipped with EDS detector (Super-X EDS system with total solid angle of 0.9 srad) was employed in the analysis to indicate the effect of the different fuels used on the PM elemental composition. The particles loaded on the TQ-filters were dissolved in ethanol and transferred into Formvar coated copper grids (200 mesh, 3.05 mm diameter, supplied from TAAB laboratories Equipment Ltd) prior to the analysis. Four distinct positions of the grids, including different agglomerate size, were inspected to determine the average composition of the different tested samples.

2.5.3: TEM and HRTEM analysis:

The needed images for the morphology and nanostructure analysis were obtained from the same Talos™ F200X S/TEM using the FEI Ceta 16M™ camera that offers an HRTEM imaging information limit up to 0.12 nm at a fast rate of 25 fps. The morphological parameters, such as radius of gyration (R_g), fractal dimension (D_f), number of primary particles (n_{po}) and their size distribution (d_{po}) were analysed through a Matlab built in digital image software following the method proposed by Lapuerta et al. [26, 27]. The nanostructure variables, such as fringe length (L_a), fringe separation distance (d_{002}), and tortuosity (T_f) were quantified following the method of Yehliu et al. [28]. $L_a > 0.5$ nm and $0.3 < d_{002} < 0.45$ nm were utilised as threshold values for this analysis in order to exclude the background effect [28]. According to the formula described by Atria et al. [29] and presented in equation 2, the particles degree of graphitization (*DOG*) is calculated as follows:

$$DOG = \frac{d002\ max - d002\ sample}{d002\ max - d002\ graphite} \qquad \text{(eq.2)}$$

Where 0.3354 nm is the interlayer spacing in graphite (d_{002} graphite) [30] and d_{002} *max* is the maximum interlayer spacing among the inspected samples.

2.5.4: Raman analysis:

Renishaw inVia Haworth 503A Raman microscopy was applied to test the PM initial graphitisation order. Argon ion laser beam with wavelength of 532 nm was implemented to test the filter samples at four distinct positions with a 50x magnification objective over the range of 800-2000 cm^{-1}. The hardware accumulation number was 15 over an exposition time of 20 seconds with an electrical source power of 6.4 μW to avoid damaging the particles nanostructure. Same as the EDX analysis, 4 spots were analysed on each filter to calculate the average spectrum.

3. Results and Discussions

3.1 Combustion analysis and gaseous emissions

As shown in table 3, longer fuel main-injection duration was needed in case of the oxygenates (D20 and T20) to maintain the same engine load condition, thus slightly higher break specific fuel consumption (BSFC) was recorded. The reduced heating value (LHV) in the oxygenated blends (Table 2) must be compensated with a higher volumetric fuel consumption to counterbalance the energy loss [31, 32]. In this context, the increased amount of the main-fuel injected lead to an extension in the diffusion combustion phase as shown in Figure 2.

Table 3: Fuel injection parameters and exhaust temperature

Fuel	Pilot injection timing (CAD BTDC)	Injection signal duration (ms)	Main injection timing (CAD BTDC)	Injection signal duration (ms)	Break specific fuel consumption BSFC (kg/kW.h)	Exhaust Temperature (°C)
Diesel	15	0.15	8	0.573 ±1	0.4082	280±2
D20	15	0.15	8	0.579 ±1	0.4209	276±2
T20	15	0.15	8	0.575 ±1	0.4201	278±2

The start of combustion (ignition delay (ID)) in common rail diesel engines correlates directly with the fuel cetane number (CN), while other physical properties are reported to have lower influence [33]. Higher CN fuels, such as T20 (TPGME CN:80), can be responsible not only for advancing the start of combustion but also lead to softer pressure and temperature profiles, as seen in Fig. 2 [34, 35]. D20 (DPGME CN: 43.9) has a similar CN compared to diesel and as a result the ID was not affected (Fig. 2), whereas the main heat release rate (HRR) peak and the exhaust temperature were slightly reduced compared to Diesel.

Concerning the gaseous emissions, increasing the oxygen content in the fuel has shown no negative impact on NOx emissions (Fig. 3) as it is commonly the case in the literature [36]. The small changes in the combustion patterns, can be one of the contributing reasons for this trend, but most likely is due to the fuels chemical properties. It is expected that the higher latent heat of vaporisation of the blends (Table 2) lowered the maximum flame temperatures and thus reduce the thermal NO formation mechanism [37]. Although the shorter ID seen in T20 combustion led to slightly higher NOx levels compared to D20, the NOx still within the error bars. It is suggested in the literature that shorter ID (as in the case of T20) can result in higher NOx

level due to an increase in the peak combustion pressure and temperature [38]. However, the direct influence of the ID on the combustion patterns cannot be fully dictated from the recorded pressure and HRR profiles, since no significant changes that allow a fair comparison was seen between the D20 and T20 fuelling. Yet, referring to the exhaust temperatures, T20 combustion results in slightly higher exhaust temperature compared to D20 and as a result higher in-cylinder temperature, which could be the reason of the increased NOx emissions.

As for the Carbon Oxides (CO) and total hydrocarbons (THC) emissions, there is slight reduction compared to the diesel. CO emissions are generally produced from the partial oxidation of the fuel when there is deficiency in oxygen. The oxygenated blends reduce the carbon mass fraction in the blend and hence reduce the CO formation mechanism [39]. Furthermore, the final CO concentrations also depend on its oxidation rate. Following the idea of An et al. [39], oxygenated fuel promotes the CO oxidation by hydroxyl (OH) radicals ($C + OH \rightarrow CO_2 + H$) . As for the HCs emissions, they generally results from the incomplete combustion of the air fuel mixture leading to unburned and partially decomposed fuel molecules [40]. The reduction shown was expected since oxygenated fuels lead to more complete combustion compared to diesel, and as a result the hydrocarbons oxidation process is promoted [31].

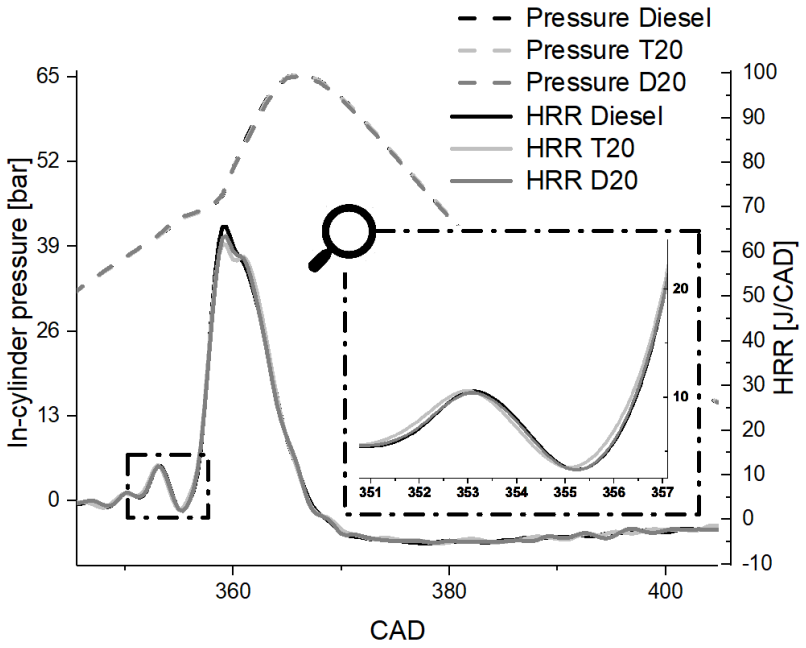

Figure 2: In-cylinder pressure, and heat release rate (HRR) from the different fuel used along with the magnified HRR region of interest

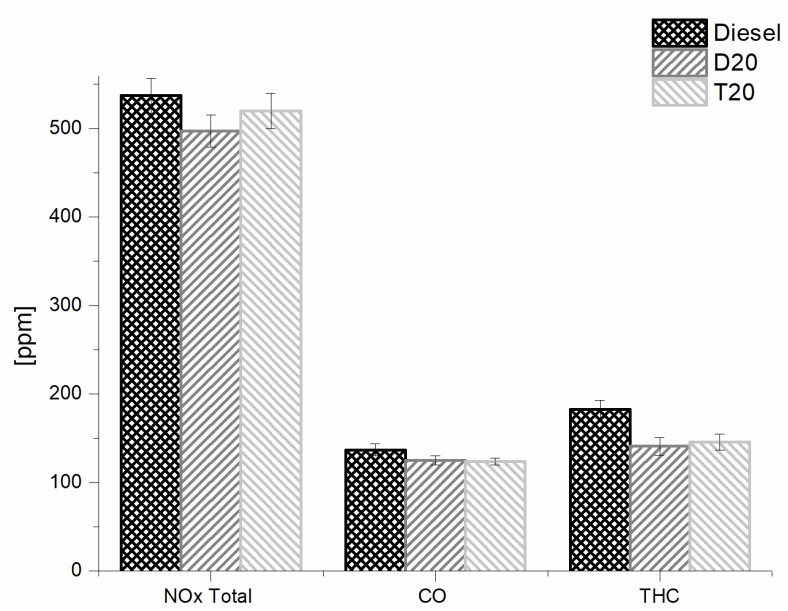

Figure 3: Gaseous emissions resulted from the different fuel blends

3.2 PM Size Distribution

In general, the C-O moieties presented in the oxygenated hydrocarbon structure are expected to survive the fuel-rich ignition phase, thereby supressing the rate of soot formation [39, 41]. Furthermore, oxygenating the fuel is expected to result in more complete combustion even in fuel rich regions along with promoting the oxidation of the already formed soot precursors [10, 11]. Consequently, it is shown that both D20 and T20 blends reduce the total particle number concentration by 25 ± 2 % and 40.3 ± 1.7 %, respectively compared to diesel (Figure 4).

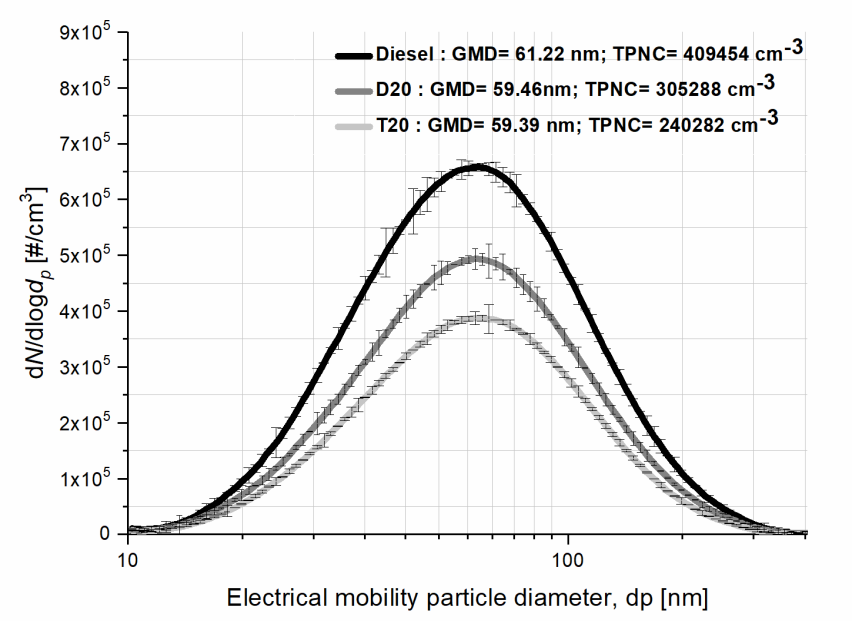

Figure 4: Particle size distribution from different blend used

Mueller [10] et al. , Burke et al. [6] and Park et al. [42] suggested that the effective PM reduction shown in case of TPGME is directly related to its atomic structure. TPGME holds four oxygen atoms evenly dispersed within the particle in such a manner that all carbon atoms are initially bonded with no more than one oxygen element. This efficient distribution ensures that all the decomposition reactions will lead to CO molecules instead of CO_2, thus inhibiting the greatest fraction of carbon atoms from contributing to soot precursor species [6].

Despite that both blends share the same oxygen content (6.5 % wt.), the particles reduction seen with D20 is smaller compared to T20. Taking into consideration that no combustion model was designed for DPGME throughout the literature and that both DPGME and TPGME share a similar structure, we can speculate that their soot reduction ability should not present significant variance. The lower soot reduction capability of D20 could be related to its higher boiling temperature (90% distillation temperature) compared to T20 (Table 2). This property indicates the presence of high molecular weight compounds that will be difficult to vaporize completely during the combustion process, favouring the production of the particulate matters [43].

3.3 Physico-Chemical Analysis of Particulate Emissions

3.3.1 Thermogravimetric Analysis

The PM collected on the TQ-filters (described in section 2.4) are mainly comprised of two compounds: (a) elemental carbon that accounts for the soot aggregates and (b) volatile components (soluble hydrocarbons, lubricants, etc.) which is adsorbed/condensed on the soot surface [24]. The fuel type significantly affects the PM composition, both oxygenates shows to produce PM with higher volatile fraction and less elemental carbon (table 4). This trend was expected since the combustion of the oxygenated blends: (a) reduces the rate of soot production (as shown in section 3.2) which results in an increase in the portion of the volatile compounds [44], (b) produces particles with higher specific surface area (shown later in section 3.3.3), which indicates an increase in the active surface in which the HCs could be adsorbed [45], (c) reduces the exhaust temperature (as shown earlier in section 3.1), which favours the condensation of the unburnt fuel on the soot surface [44].

Table 4: Start of oxidation and ignition temperature along with the corresponding volatile fraction of the soot resulted from the different blend combustion.

Soot origin	Start of oxidation (^{o}C)	Ignition temperature (^{o}C)	Volatile fraction (%)
Diesel	378.4 ± 3	497 ± 1	70.53 ± 2
D20	360 ± 2.5	480 ± 3	72.8 ± 1
T20	360 ± 2.5	480 ± 4	80.95 ± 4

Inspecting the soot weight loss curve (table 4 and Figure 5), particles resulted from both D20 (S_{D20}) and T20 (S_{T20}) show to start oxidising at a lower temperature (360 ± 2.5 ^{o}C) compared to diesel soot (S_D) (378.4 ± 3 ^{o}C). The corresponding mass loss rate (dm/dt) was also plotted in figure 5 to determine the particles ignition

temperature (Ti), usually defined as the temperature where the maximum mass loss rate occurs (Lower the Ti, higher the reactivity) [13, 25]. As shown in figure 5, both S_{D20} and S_{T20} present a lower Ti (480 ± 1.3 °C) compared to S_D (497 ± 1 °C), indicating that oxygenated fuel blends produce particles with higher oxidative potential compared to the neat diesel combustion.

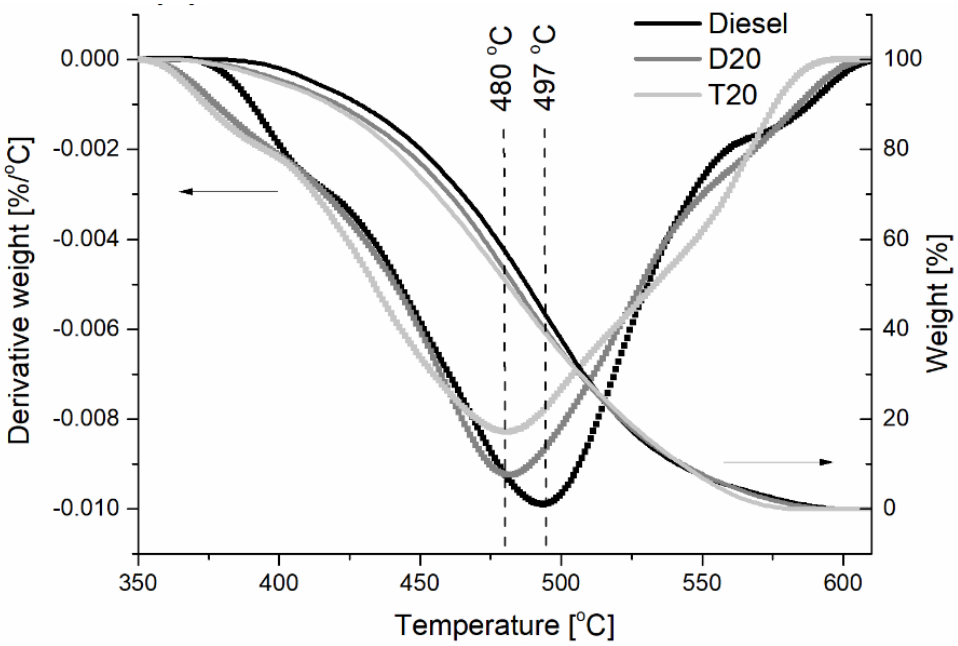

Figure 5: Soot weight variation and mass loss rate for the different fuels

To further investigate the particles reactivity, the soot activation energy (Ea) was calculated following the method stated earlier in section 2.5.1. In the calculation, the temperature range that corresponds to the soot conversion rate of 10% to 50% was considered, since it results in the most linear trend (as shown by the correlation coefficient R^2 in Figure 6) [24]. S_{T20} shows to be the most reactive with a corresponding Ea of 100 kJ/mol followed by S_{D20} with Ea = 115.2 kJ/mol and S_D with Ea = 119.36 kJ/mol. As a first step of the analysis, the difference shown along the particles reactivity could be clarified following the particles volatile fraction. Although the volatiles were evaporated before launching the oxidation process, the devolatilization of these compounds is reported to increase the particles reactivity through raising the soot porosity (micropores opening), providing an increase in the internal surface area in which oxygen could penetrate and react [46]. This theory perfectly fits our outcomes where S_{T20}, presenting the highest volatile fraction, lead to the highest reactivity (lowest Ea), followed by S_{D20} and S_D respectively.

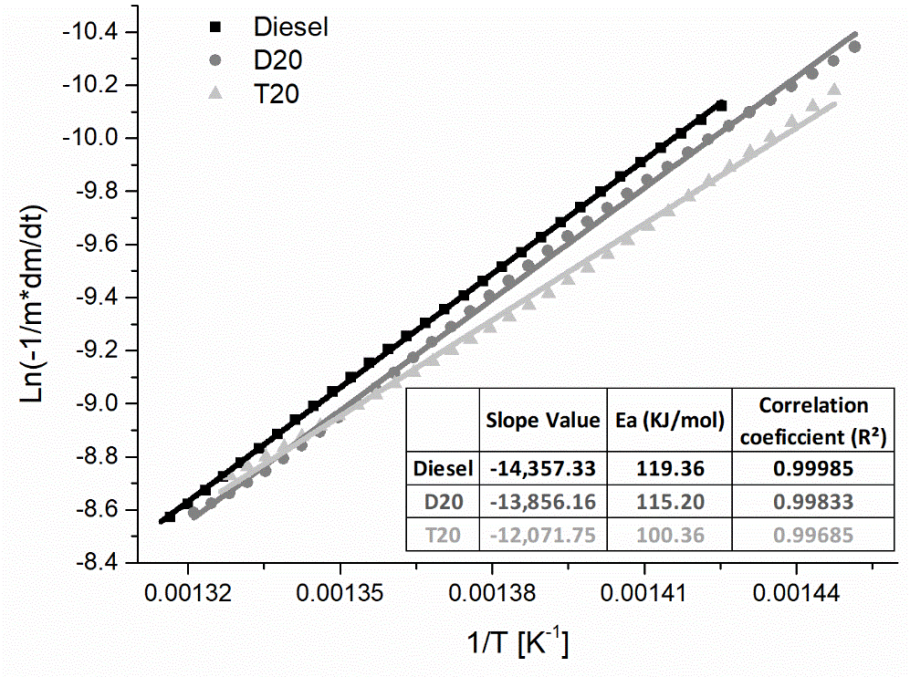

Figure 6: Effect of fuel type on the soot activation energy extracted from the corresponding Arrhenius-plot

With respect to the above soot oxidation kinetics, it is quite evident that the oxygenation of the diesel fuel can shift the diesel particulate filter (DPF) regeneration process towards lower temperatures [47]. In an effort to understand the detected reactivity, a more detailed examination of the different physical and chemical soot properties is performed in the following sections of the paper.

3.3.2 PM elemental composition

S/TEM-EDX has been employed in this study to analyse the chemical composition of the collected PM samples. As shown in Figure 7, the elementary analysis of the PM includes oxygen, carbon, sulphur as well as ash content (aluminium and Zinc). However, this method cannot detect the hydrogen (atomic number Z=1) levels since light elements with Z<11 cannot be analysed by the EDX method [48]. To collect the same filter PM loading, sample collection time varies between the different fuel blends in the following order T20>D20>ULSD, confirming the SMPS results since T20 presents the lowest PM presence in the exhaust, followed by D20 and Diesel respectively.

- Ash content:

Zinc (Zn) and Aluminium (Al) were indicated as the major ash source in the PM studied in this work. Zinc is considered as an active catalyst that enhances the oxidative reactivity of the particles (earlier and faster oxidation) while Aluminium is reported to have less influence [49, 50]. These type of metals are generated from inorganic elements in the fuel, lubrication oil and engine wear [13]. Despite the fact that the PM collection duration was longer in case of the oxygenated blends, their ash content (8-9 %) is slightly lower compared to the diesel case (12%). DPGME and TPGME present pure oxygenated hydro-carbons where no metals such as Ca, S and P-bearing components can be found as it is the case in biodiesel [51]. These compounds (DPGME and TPGME) dilute the inorganic elements concentration in diesel fuel without adding

any ash precipitations. Reduction in the ash content of the particles help in sustaining the DPF service life since ash accumulation increases the system backpressure, leading to less efficient combustion and higher fuel penalties [52]. Beside the microstructural difference that will be explained later in section 3.3.4, the reduction in the catalytic active materials (ash components) present a valid reason to clarify the slight difference shown along the starting oxidation temperature shown earlier in section 3.3.1 (Table 4).

- Sulphur:

Small amounts of sulphur (1.5 %) were detected in the diesel PM sample. It can be attributed to the unburned fuel portion that is condensed on the soot surface. Oxygenates addition reduces the sulphur concentration in the fuel blend, thus smaller portion is expected to accumulate on the soot periphery. It is believed that this reduction was significant up to a level that wasn't detectable by the EDX analyser.

- Carbon:

PM carbon content was shown to significantly decrease in case of the oxygenated blends (55%-D20, 50%-T20) with respect to the conventional diesel (62%). This reduction confirms the influence of the molecular oxygen (C-O moieties) on the soot formation mechanism described earlier in section 3.2. Furthermore, the in-cylinder soot oxidation promotion described in case of the oxygenated blends is not only expected to decrease the final soot mass but also reduce the mass of carbon grouped in the particles [53].

- Oxygen:

Oxygen concentrations are greater in case of blended fuels with different grades, 9 % for D20 and 13 % for T20 compared to diesel. Oxygen fraction increment in case of the oxygenates is resulted from the condensation of the unburned fuel (containing oxygen compounds) on the soot periphery and support the presence of a higher fraction of surface bond-oxygen functional groups [54]. As for the difference shown between D20 and T20, it was expected since T20 present higher volatile fraction compared to D20 (section 3.3.1), therefore higher portion of oxygenated compounds is expected to be accumulated on the soot surface.

The elemental composition shown for diesel PM (C and O) in that analysis correlates with previous findings by Salamanca et al. [55]; as for D20 and T20 blends no study in the literature has reported its elemental composition. The incorporation of the greater amounts of oxygen functional groups is expected to enhance the soot oxidation rate by favouring the internal burning mode during the oxidation process, as suggested by Song et al. [54].

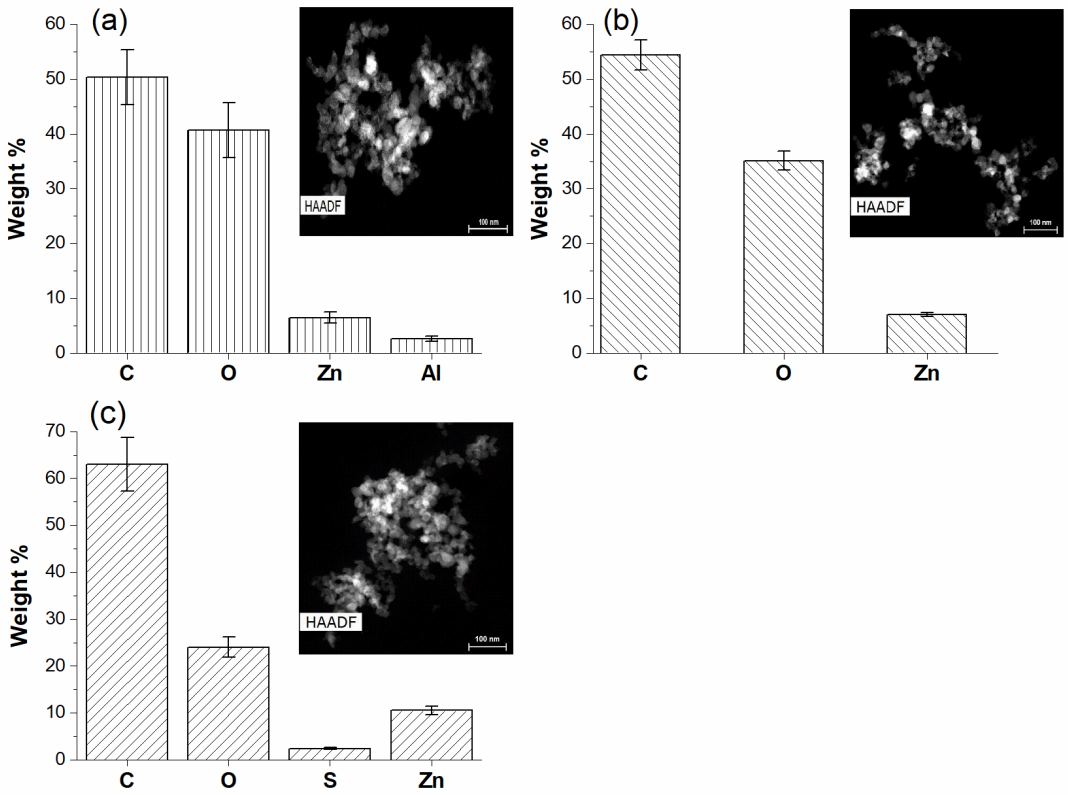

Figure 7: Elemental composition of the PM samples calculated from the EDX- Analysis, (a) Diesel, (b) D20, (c) T20

3.3.3 PM Morphological Analysis

All the micrographs were set to have the same magnification scale of 100 nm and the samples were collected at the same exhaust sampling point. All the aggregates present the typical morphology of diesel PM, showing nearly spherical primary particles blended together to form a stretched chain like structure (Figure 7).

The primary particles size (d_{po}) distribution was plotted in Figure 8 by selecting around 350 particles (approximately 30 TEM images were analysed) in each case. Oxygenated blends tend to supress the rate of soot inception and promote the oxidation of the already formed particulates, as discussed earlier in section 3.2. Consequently, fewer number of primary particles (n_{po}) was presented in the agglomerates derived from D20 and T20 blends, and their size (d_{po}) shows to be 17.8-25 % smaller than diesel (Figure 8 and 9). As a result, radius of gyration (R_g) of the particles was shown to slightly decrease from 70 nm in case of diesel to 64-65 nm in case of D20 and T20 respectively (Figure 9).

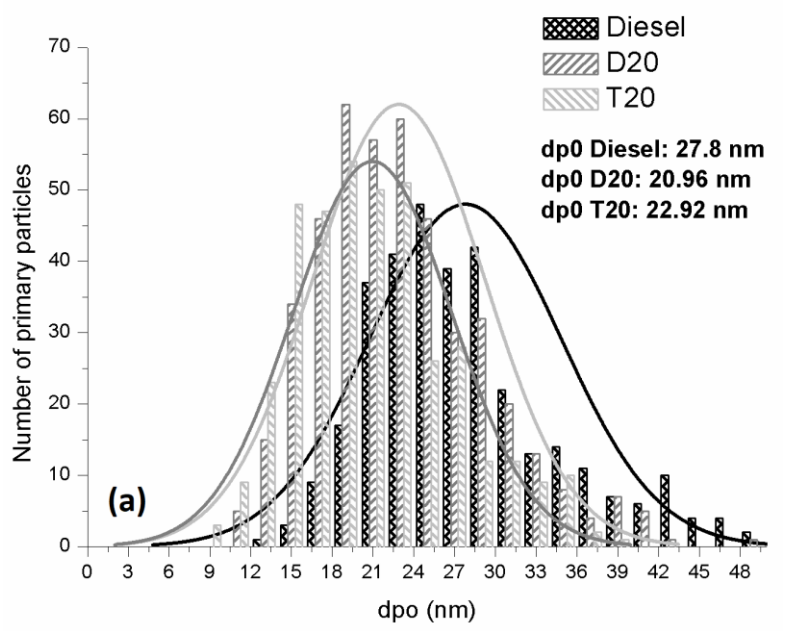

Figure 8: Primary particles size distributions resulted from the combustion of diesel, D20, and T20 fuel blends

Assuming that the soot shape is perfectly spherical and its density is 1850 kg/m^3, the specific surface area (SSA) was calculated following the method proposed by Lapuerta et al. [56]. Following the reduction shown along d_{po}, the SSA of the primary particles increases from 115 g/m^2 in case of S_D to 140 and 155 g/m^2 for S_{D20} and S_{T20} respectively. Higher SSA (smaller d_{po}) indicates that the resulted particles are more vulnerable to oxygen attack, and as a result their oxidative reactivity should be improved [56, 57]. Other authors suggested that the correlation between the primary particle size and the particles reactivity is not always consistent [13, 58]. Considering the reduction shown along d_{po} in case of the oxygenates and the corresponding higher oxidative reactivity reported previously in section 3.3.1, this work reflects the existence of a positive correlation between these two parameters and confirms the theory stated in ref. [56, 57]. The fractal dimension (D_f) is considered as a metric scale to estimate the structure of the resulted PM aggregates [59]. In general, higher particle concentration enhances the collision phenomena between the particles and results in aggregates having lower fractal dimension (more chain like structure) [60]. Despite the lower levels of particles generated in the case of the oxygenates, D_f was approximately 7% lower compared to diesel (Figure 9). This is attributed to the promoted oxidation of the already formed agglomerates during the combustion of the oxygenated blends [16, 61]. Therefore, it is expected that the resulted particulates would be more efficiently trapped in the DPF due to their chain-like structure [61].

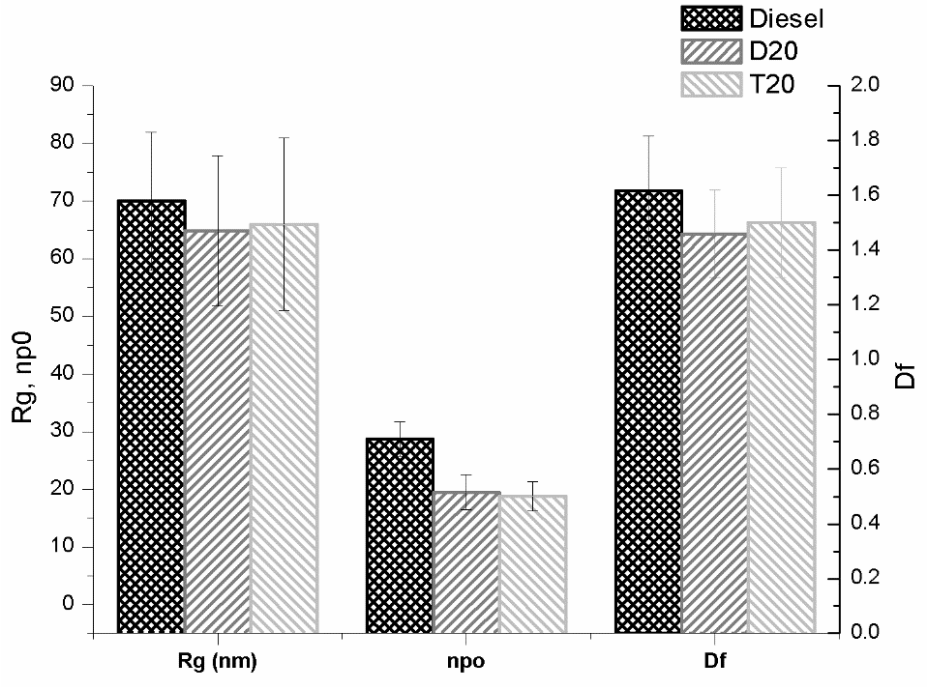

Figure 9: Effect of fuel type on radius of gyration (R_g), number of primary particles (n_{po}) and fractal dimension (D_f)

3.3.4. Primary particle nanostructure

Primary particle structure analysis was conducted using the same magnification scale of 20 nm precision. Figure 10 shows the original grey scale HRTEM images where the region of interest is processed as skeleton function to clearly show their structural details. All the particles inspected present two distinct parts as a main structure: outer shell consisting of ordered PAH layers, so called "fringes", that surrounds an inner part, so called "particle core", where unsymmetrical arrangement for the graphene layers can be seen.

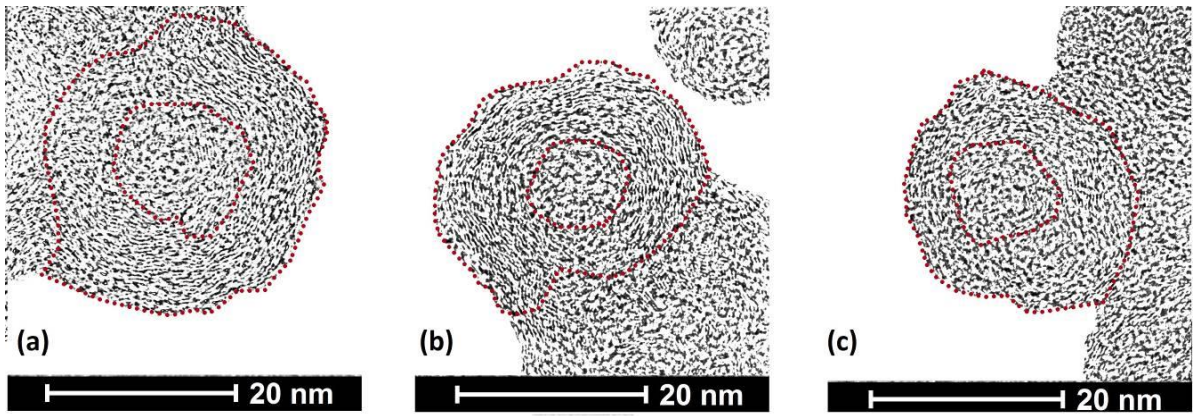

Figure 10: HR-TEM micrograph presenting the primary particle structure resulted from the combustion of the different fuel used, (a) diesel (b) D20 (c) T20

The carbon atoms located in the basal plane have lower reactivity compared to the edge site position. The accessible number of the carbon layers in the edge sites can be predicted by analysing the primary particles nanostructure parameters stated earlier in section 2.5.3 [62]. The resulted variables are presented in Figure 11 and 12 as a normal distribution to show the variations in detail between the different particles inspected.

- ***Fringes Length (L_a) and Fringe Tortuosity (T_f):***

Oxygenated fuels tend to produce particles characterised by shorter fringe length (L_a) and higher tortuosity (T_f) compared to diesel [58, 63]. In general, short L_a highlights the presence of greater number of carbon atoms in the edge sites, in other words more reactive particles [62, 64]. Higher T_f (more curved fringes) impose the bond/ring strain (distort bonds from their ideal values) which increases the reactivity of the carbon atoms located in the basal plane since their atomic orbitals overlap and their electronic resonance stabilization is reduced [62, 64]. Therefore, the C-C bonds are weakened and become more vulnerable to the oxidative attack [62]. Higher levels of T_f was predicted to increase the possibility of breaking the outer layer into smaller fringes during the oxidation process, thus enhancing the reactivity of the particles [56]. Van Der Wal et al. [62] proved that T_f present more influential effect compared to L_a in term of increasing the PM reactivity.

In this work, L_a present a non-linear trend between the different particles, S_{T20} comprise shorter layers compared to the diesel case while S_{D20} tend to present longer layers (i.e. less reactive particle) (Figure 11). This result supports the higher reactivity shown along S_{T20} compared to S_{D20}, but in the same time contradicts the fact that both particles are still more reactive than diesel particles. In this context, it can be clearly stated that the fringes length (L_a) cannot be considered as a critical parameter that dictates the PM oxidative behaviour and other factors should be accounted for a more adequate analysis.

Oppositely to L_a, both blends tend to produce particles with higher T_f compared to diesel. This trend was expected since the combustion of the oxygenated blends lead to the formation of smaller primary particles compared to diesel, thus the carbon layers are likely to be more stretched (more curved) [56]. Furthermore, the elevated amounts of the PM surface oxygen groups shown earlier in case of the oxygenates (section 3.3.2) could be another possible reason for that trend. Man et al. [25] reported that the oxygen functional groups on the soot surface can "change the connection types between the carbon atoms in a graphene layer", leading to more curved fringes.

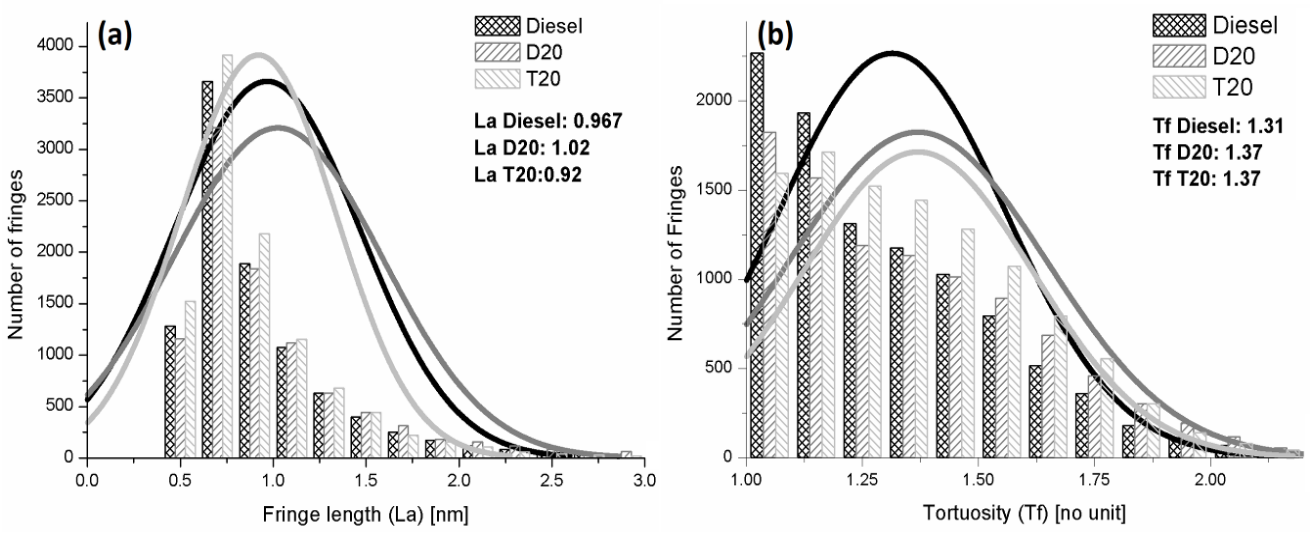

Figure 11: Nanostructure parameters of the inspected particles: (a) fringe length (L_a), (b) tortuosity (Tf)

- ***Fringes Separation Distance (d_{002}) and Degree of Graphitisation (DOG):***

Higher fringes separation distances (d_{002}) are reported in the literature to enhance the particles oxidative reactivity by facilitating the access of the oxygen to the carbon edge sites [63]. It is commonly accepted throughout the literature that the combustion of oxygenated diesel blends (especially biodiesel) produce particles with larger d_{002} compared to the conventional diesel [65, 66]. Combustion temperature and soot residence time constitute a governing factor that dictates the particles degree of graphitisation [58]. In general, soot produced under high in-cylinder temperatures are expected to have higher *DOG* and consequently possess lower active surface area (lower reactivity) [58]. In contrast, Lapuerta et al. reported that the variation in the particles structural order depends more on the fuel type rather than on the combustion temperature [56].

Despite the lower exhaust temperature from the combustion of the oxygenated blends (see section 3.1), thus lower in-cylinder temperature, the resulted PM present shorter d_{002} between its graphene layers (Fig. 12). This reveals that oxygen borne fuels produce particles with more ordered graphite-like structure compared to diesel, which was further confirmed by calculating their *DOG* following the equation stated earlier in section 2.5.3. The particles DOG changes in the following order: D20 ~ 0.525 > T20 ~ 0.505 > Diesel ~ 0.439. These findings confirm Lapuerta's theory [56], proving that the particle *DOG* is more fuel dependant rather than engine dependant. Furthermore, the initial higher *DOG* in case of the oxygenates did not negatively affect the particles reactivity during the oxidation process (Figure 5), thereby highlighting that the initial graphitic order is not the only dominant factor that determines the oxidative behaviour of the particles. However, it could be speculated that the negligible difference between $S_{D20,\ T20}$ and S_D regarding the starting oxidation temperature (as seen in section 3.3.1) may be also influenced by that factor.

Following our results, the fringes tortuosity seems to be the most critical nano-structural parameter influencing the particles reactivity in our analysis, a trend that was suggested earlier by Lapuerta et al. [56].

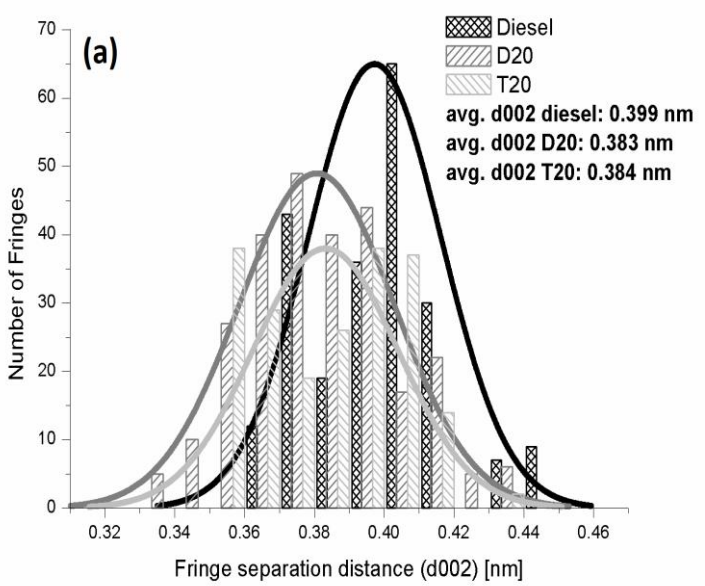

Figure 12: Particles fringe separation distance (d_{002})

3.3.5 Graphitic structure order

The particles structural variance indicated earlier by the HRTEM analysis was further investigated by the aim of Raman spectroscopy. The obtained spectra was first corrected by a linear baseline and then de-convoluted into 3 Lorentzian shape bands (D4 ~ 1200 cm^{-1}, D1 ~ 1350 cm^{-1} and G ~ 1580 cm^{-1}) and 1 Gaussian band (D3 ~ 1500 cm^{-1}) based on the approach by Ess et al. [67] (Figure 13). In general, differences between the intensities, area and full width at half maximum (FWHM) of the different resulted bands refer to different structural orders in the basal plane of the graphene layers [56]. Among the examined bands, G and D1 present the most intense peaks; G attribute to the ideal graphitic structure while D1 refers to disorder in the edges of the layers.

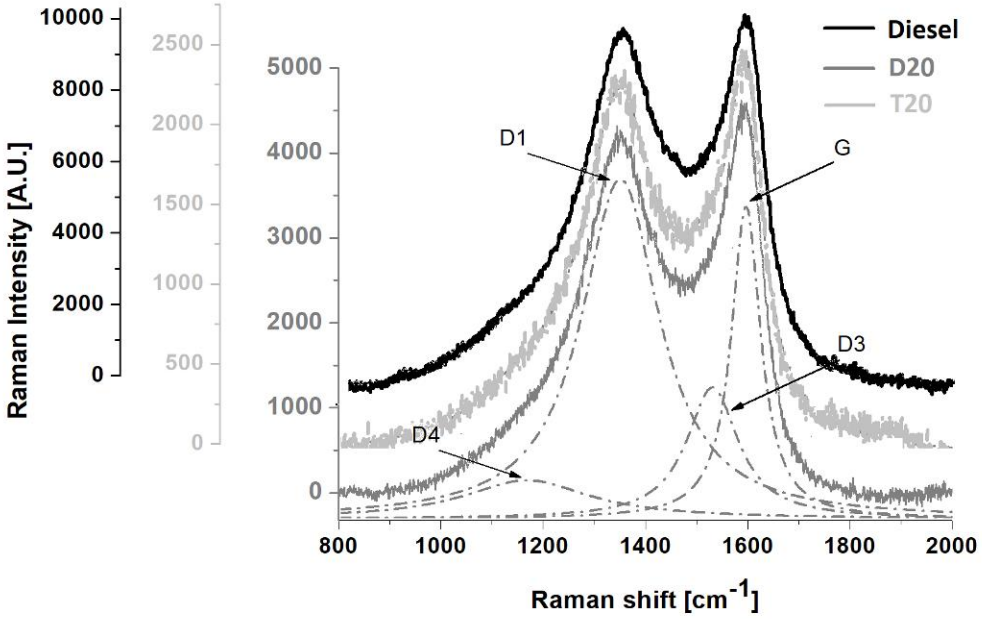

Figure 13: Raman spectra of diesel soot with its corresponding Lorentzian curve fitting, Diesel, D20 and T20 spectrum

The intensity and area ratio of D1 with respect to G ($I_{D1}/I_{G,}$ A_{D1}/A_G), next to the FWHM of D1 present an indicator to quantify the density of the edges sites and the crystalline sizes distribution [58]. These indicators are considered as useful parameters to interpret the particles *DOG* [13]. Seong et al. [68] considered these ratios as an important factor that rule the particles oxidative reactivity, lower ratios correlates with a lower reactivity. As shown in table 5, soot originated from oxygenated blends presents lower FWHM D1, I_{D1}/I_G and A_{D1}/A_G ratio compared to diesel. These results agree with the reduction shown along d_{002} in section 3.3.4 and confirms that the layers of the particles tend to be more ordered in case of the oxygenates. These results did not follow the theory mentioned earlier in ref. [68] since, as stated in section 3.3.4, fringes tortuosity (which cannot be identified by Raman analysis) is the only nanostructure variable dictating the oxidative behaviour in that work. Furthermore, D3 results from amorphous carbon, i.e. organic molecules, fragments or functional group. No significant changes were detected along that band between the different tested samples. D4 is directly related to the vibration caused by the single or double carbon-carbon bonds (C-C, C=C)

presented in polyene-like structures which indicates disorder in the graphitic lattice [69]. Same as D1, A_{D4}/A_G shows to slightly decrease in case of oxygenates confirming the higher *DOG* reported earlier.

Table 5: FWHM D1, I_{D1}/I_G, A_{D1}/A_G, A_{D3}/A_G, A_{D4}/A_G for the soot from the combustion of Diesel, D20 and T20 blends

Soot origin	FWHM D1	I_{D1}/I_G	A_{D1}/A_G ratio	A_{D3}/A_G	A_{D4}/A_G
Diesel	186 ± 0.5	1.158 ± 0.025	2.95 ± 0.03	0.75 ± 0.013	0.53 ± 0.04
D20	184 ± 0.3	1.1119 ± 0.012	2.83 ± 0.06	0.77 ± 0.023	0.45 ± 0.06
T20	182 ± 0.2	1.088 ± 0.021	2.75 ±0.05	0.78 ± 0.024	0.32 ± 0.05

4. Summary of results

The several analytical techniques implemented to characterise the different PM properties are presented in the 1st column of Figure 14. The effect of both D20 and T20 blends on the different particles physico-chemical properties (morphological, nano-structural and elemental) is shown in the 2nd column of the graph. Furthermore, the way with which every physico-chemical property influences the rest of the studied properties (i.e. higher d_{002} lead to higher *DOG*) is presented through the arrows sketched on the both sides of the 2nd column.

The general impact of these properties on the particles oxidative behaviour, as it is commonly reported in the literature, is shown in the 3rd column of the graph to clearly identify the properties that correlate with the enhanced oxidative potential recorded in that work. As a summary, the different physico-chemical properties inspected were qualitatively classified into two main groups: "**Factors with major influence on the oxidative behaviour of the particles**" and "**Factors with minor influence on the oxidative behaviour of the particles**".

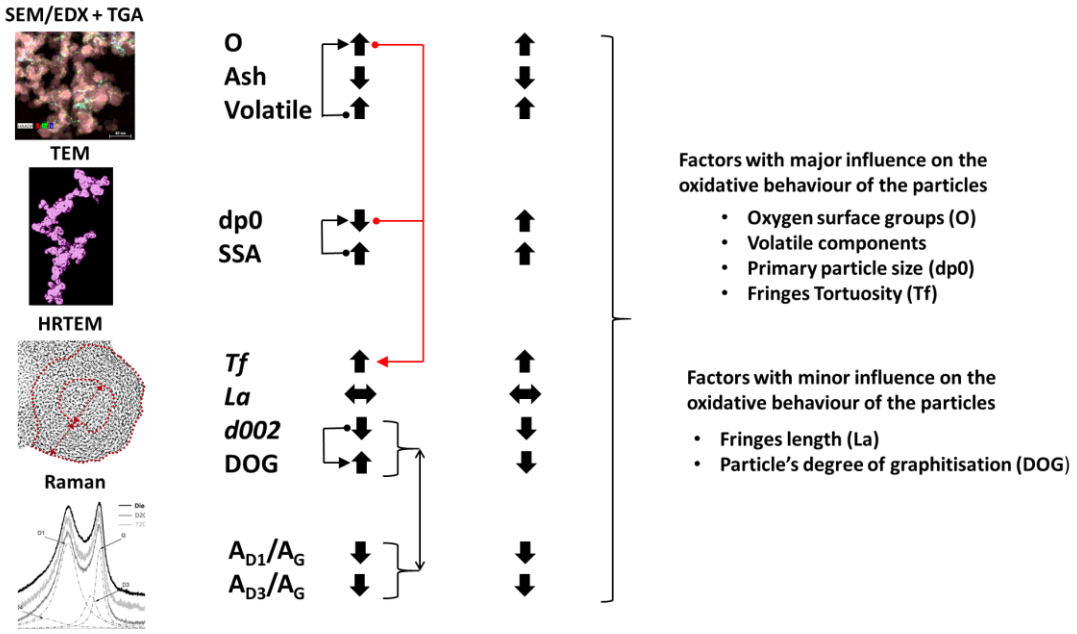

Figure 14: Summary of the different physico-chemical parameters affecting the particles reactivity

Conclusions

The effect of adding di and tri-propylene glycol methyl ether to diesel (6.5 w.t % oxygen content) on the gaseous emissions, sooting tendency, and oxidative reactivity of the particulate matters along with their physico-chemical characteristics was investigated in this study. Increasing the fuel oxygen content shows no negative impact on the NOx production for both blends, while T20 fuelling shows to be more effective than D20 in PM reduction. The particles resulted from the oxygenated fuels shows to be more reactive compared to diesel but the relationship between the particles physico-chemical properties and reactivity was quite complex.

Particles morphology displays significant modifications, both blends results in aggregates with more chain-like structure that includes fewer number and smaller primary particles compared to diesel. Inspecting the particles carbon layers, oxygenated fuels show to slightly influence the fringes length (L_a) but tend to significantly elevate their tortuosity levels (T_f). Unexpectedly, both Raman and HRTEM analysis highlight that glycol ether blends increase the particles initial graphitisation order, which contradicts the higher reactivity recorded. In addition, lower ash precipitations and higher oxygen content was detected through the elemental analysis of the PM.

Given the results of this work, it appears that the initial carbon layers length (L_a) and particles graphitisation degree present no clear indication in presuming the particles oxidative behaviour, as it is the case in the literature. However, initial primary particle size and surface oxygen group present the major role in dictating the particles reactivity, since beside their positive impact on the oxidation mechanism, they both influence the fringes tortuosity (T_f), whose been considered as the most critical parameter governing the reactivity shown in that analysis.

This work shows that apart from effectively reducing the PM emissions, glycol ether blends combustion could also help in decreasing the severity of the DPF regeneration process (i.e. lower soot activation energy) and increase the filter lifespan (i.e. lower soot ash content) without affecting its filtration efficiency (i.e. soot with chain-shape morphology).

Acknowledgment

Innovative UK (The Technology Strategy Board, TSB) and EPSRC are acknowledged for supporting this work with the projects CREO ref 400176/149 and EP/G038139/1, respectively. F.J. Martos expresses thanks to the government of Spain for supporting his research stay with reference PRX15/00256 at University of Birmingham. With thanks to Advantage West Midlands and the European Regional Development Fund, funders of the Science City Research Alliance Energy Efficiency project−a collaboration between the Universities of Birmingham and Warwick.

References

1. Silverman, D.T., et al., *The Diesel Exhaust in Miners study: a nested case-control study of lung cancer and diesel exhaust.* J Natl Cancer Inst, 2012. **104**(11): p. 855-68.

2. Gonzalez, M.A., et al., *Oxygenates screening for AdvancedPetroleum-Based Diesel Fuels Part 2: The Effect of Oxygenate Blending Compounds on Exhaust Emission.* SAE, 2001(2001-01-3632).
3. Gogoi, B., et al., *Effects of 2,5-dimethylfuran addition to diesel on soot nanostructures and reactivity.* Fuel, 2015. **159**: p. 766-775.
4. da Silva, G.P., M. Mack, and J. Contiero, *Glycerol: a promising and abundant carbon source for industrial microbiology.* Biotechnol. Adv., 2009. **27**(1): p. 30-9.
5. Yu, Z., et al., *A new route for the synthesis of propylene oxide from bio-glycerol derivated propylene glycol.* Chem. Commun., 2009(26): p. 3934-6.
6. Burke, U., W.J. Pitz, and H.J. Curran, *Experimental and kinetic modeling study of the shock tube ignition of a large oxygenated fuel: Tri-propylene glycol mono-methyl ether.* Combust. Flame, 2015. **162**(7): p. 2916-2927.
7. Guo, H., S. Liu, and J. He, *Performances and Emissions of New Glycol Ether Blends in Diesel Fuel Used As Oxygenated Fuel for Diesel Engines.* J. Energy Eng., 2016. **142**(1:04015003): p. 1-7.
8. Gómez-Cuenca, F., M. Gómez-Marín, and M.B. Folgueras-Díaz, *The influence of propylene glycol ethers on base diesel properties and emissions from a diesel engine.* Energ. Convers. Manage., 2013. **75**: p. 741-747.
9. Natarajan, M., et al., *Oxygenates for Advanced Petroleum-Based Diesel Fuels: Part 1. Screening and Selection Methodology for the Oxygenates.* SAE, 2001(2001-01-3631).
10. Mueller, C.J., et al., *Effects of Oxygenates on Soot Processes in DI Diesel Engines: Experiments and Numerical Simulations.* SAE Technical Paper, 2003(2003-01-1791).
11. Dumitrescu, C.E., C.J. Mueller, and E. Kurtz, *Investigation of a tripropylene-glycol monomethyl ether and diesel blend for soot-free combustion in an optical direct-injection diesel engine.* Appl. Therm. Eng., 2016. **101**: p. 639-646.
12. Hilden, D.L., J.C. Eckstrom, and L.R. Wolf, *The Emissions Performance of Oxygenated Diesel Fuels in a Prototype DI Diesel Engine.* SAE, 2001(2001-01-0650).
13. Mühlbauer, W., et al., *Correlations between physicochemical properties of emitted diesel particulate matter and its reactivity.* Combust. Flame, 2016. **167**: p. 39-51.
14. Leidenberger, U., et al., *Experimental studies on the influence of diesel engine operating parameters on properties of emitted soot particles.* Combust. Sci. Technol. , 2012. **184**: p. 1-15.
15. Liati, A., et al., *Variations in diesel soot reactivity along the exhaust after-treatment system, based on the morphology and nanostructure of primary soot particles.* Combust. Flame, 2013. **160**(3): p. 671-681.
16. Fayad, M.A., et al., *Manipulating modern diesel engine particulate emission characteristics through butanol fuel blending and fuel injection strategies for efficient diesel oxidation catalysts.* Appl. Energy, 2017. **190**: p. 490-500.
17. Shell Chemicals. *Methyl DIPROXITOL specification sheet*. 2007; Available from: http://webcache.googleusercontent.com/search?q=cache:I72Ijn_Y6n0J:www.alchemchemical.com/products.html%3Ffile%3Dtl_files/product_documents/MSDS/shell/glycol-ether-dpm-tech-07-01-01.pdf+&cd=2&hl=en&ct=clnk&gl=uk.
18. Park, S., et al., *Development of a reduced tri-propylene glycol monomethyl ether-n-hexadecane-poly-aromatic hydrocarbon mechanism and its application for soot prediction.* IJER, 2016.
19. Sattler, E., *Comparing Methods to Determine Cetane Ratings of Fuel Blends.* RDECOM, 2009(0704-0188).
20. Yanowitz, J., R.L.M. M.A. Ratcliff, and J.D. Taylor, and M.J. Murphy, *Compendium of Experimental Cetane Numbers.* NREL, 2014(TP-5400-61693).
21. Jacobus, P. and M. Frijters, *Fuel Composition Impact On Heavy Duty Diesel Engine Combstion & Emissions.* Eindhoven University of Technology, 2012. **PhD Thesis**.
22. Bogarra, M., et al., *Study of particulate matter and gaseous emissions in gasoline direct injection engine using on-board exhaust gas fuel reforming.* Appl. Energy, 2016. **180**: p. 245-255.
23. Ma, Z., et al., *Effects of Diesel Oxidation Catalyst on Nanostructure and Reactivity of Diesel Soot.* Energy Fuels, 2014. **28**(7): p. 4376-4382.
24. Wang, C., et al., *Fuel Effect on Particulate Matter Composition and Soot Oxidation in a Direct-Injection Spark Ignition (DISI) Engine.* Energy Fuels, 2014. **28**(3): p. 2003-2012.

25. Man, X.J., et al., *Effect of Waste Cooking Oil Biodiesel on the Properties of Particulate from a DI Diesel Engine.* Aerosol Sci.Technol., 2015. **49**(4): p. 199-209.
26. Lapuerta, M., R. Ballesteros, and F.J. Martos, *A method to determine the fractal dimension of diesel soot agglomerates.* J Colloid Interface Sci, 2006. **303**(1): p. 149-158.
27. Lapuerta, M., F.J. Martos, and G. Martin-Gonzalez, *Geometrical determination of the lacunarity of agglomerates with integer fractal dimension.* J Colloid Interface Sci, 2010. **346**(1): p. 23-31.
28. Yehliu, K., R.L. Vander Wal, and A.L. Boehman, *Development of an HRTEM image analysis method to quantify carbon nanostructure.* Combust. Flame, 2011. **158**(9): p. 1837-1851.
29. J.V. Atria, F.R.J., H.H. Schobert, *Structural Ordering of Pennsylvania Anthracites on Heat Treatment to 2000-2900 °C.* Energy Fuels, 2002. **16**: p. 1343-1347.
30. Seehra, M.S.P., *X-ray Diffraction, Thermal Expansion, Elecrical Conductivity, And Optical Microscopy Studies Of Coal-Based Graphites.* Carbon, 1993. **31**(4): p. 557-564.
31. Ren, Y., et al., *Combustion and emissions of a DI diesel engine fuelled with diesel-oxygenate blends.* Fuel, 2008. **87**: p. 2691-2697.
32. Kousoulidou, M., et al., *Biodiesel blend effects on common-rail diesel combustion and emissions.* Fuel, 2010. **89**(11): p. 3442-3449.
33. Lapuerta, M., O. Armas, and J. Rodriguezfernandez, *Effect of biodiesel fuels on diesel engine emissions.* Prog Energy Combust Sci. , 2008. **34**(2): p. 198-223.
34. Schmidt, K. and J. Van Gerpen, *The Effect of Biodiesel Fuel Composition on Diesel Combustion and Emissions.* SAE, 1996. **961086**.
35. Kidoguchi, Y., et al., *Effects of fuel cetane number and aromatics on combustion process and emissions of a direct-injection diesel engine.* SAE, 2000. **21**: p. 469-475.
36. Hoekman, S.K. and C. Robbins, *Review of the effects of biodiesel on NOx emissions.* Fuel Process. Technol., 2012. **96**: p. 237-249.
37. Lei, J., Y. Bi, and L. Shen, *Performance and emission characteristics of diesel engine fueled with ethanol-diesel blends in different altitude regions.* J. Biomed. Biotechnol., 2011. **2011**: p. 417421.
38. O.C. Chukwuezie, N.R.N., S.N. Asoegwu and K.N. Nwaigwe, *Cetane Number Effect on Engine Performance and Gas Emission: A Review.* AJER, 2017. **6**(1): p. 56-67.
39. An, H., et al., *Modeling study of oxygenated fuels on diesel combustion: Effects of oxygen concentration, cetane number and C/H ratio.* Energy Convers. Manag, 2015. **90**: p. 261-271.
40. SITSHEBO, S.W.T., *HC-SCR of NOx emissions over Ag/Al2O3 catalysts using diesel fuel as a reductant.* University of Birmingham, 2010. **PhD Thesis**.
41. Westbrook, C.K., W.J. Pitz, and H.J. Curran, *Chemical Kinetic Modeling Study of the Effects of Oxygenated Hydrocarbons on Soot Emissions from diesel engines.* J. Phys. Chem., 2006. **110**: p. 6912-6922.
42. Park, W., et al., *The effect of oxygenated fuel properties on diesel spray combustion and soot formation.* Combust. Flame, 2017. **180**: p. 276-283.
43. Cataluña, R. and R. da Silva, *Effect of Cetane Number on Specific Fuel Consumption and Particulate Matter and Unburned Hydrocarbon Emissions from Diesel Engines.* Journal of Combustion, 2012. **2012**: p. 1-6.
44. Wei, L., C.S. Cheung, and Z. Ning, *Influence of waste cooking oil biodiesel on the nanostructure and volatility of particles emitted by a direct-injection diesel engine.* Aerosol Sci.Technol., 2016. **50**(9): p. 893-905.
45. Ballesteros, R., et al., *Speciation of the semivolatile hydrocarbon engine emissions from sunflower biodiesel.* Fuel, 2008. **87**(10-11): p. 1835-1843.
46. Betancourt, E.J.B., *Impact of oxygenated fuel on sooting tendency and soot oxidative reactivity with application to biofuels.* The Pennsylvania State University, 2014. **PhD thesis**.
47. Bhardwaj, O.P., et al., *Fuel formulation effects on the soot morphology and diesel particulate filter regeneration in a future optimized high-efficiency combustion system.* IJER, 2017. **18**(5-6): p. 591-605.
48. Australian Micrpscopy and Microanalysis Research Faculty. *Quantitative EDS X-ray microanalysis using SEM*. 2014; Available from: http://www.ammrf.org.au/myscope/analysis/eds/quantitative/.

49. Moldanová, J., et al., *Physical and chemical characterisation of PM emissions from two ships operating in European Emission Control Areas.* Atmos. Meas. Tech., 2013. **6**(12): p. 3577-3596.
50. López-Suárez, F.E., A. Bueno-López, and M.J. Illán-Gómez, *Cu/Al2O3 catalysts for soot oxidation: Copper loading effect.* Appl. Catal., B, 2008. **84**: p. 651-658.
51. Liati, A., et al., *Microscopic investigation of soot and ash particulate matter derived from biofuel and diesel: implications for the reactivity of soot.* J. Nanopart. Res., 2012. **14**(11).
52. Sappok, A. and V. Wong, *Ash Effects on Diesel Particulate Filter Pressure Drop Sensitivity to Soot and Implications for Regeneration Frequency and DPF Control.* SAE Int. J. Fuels Lubr. , 2010. **3(1)**.
53. Xi, J. and B.J. Zhong, *Soot in Diesel Combustion Systems.* Chem. Eng. Technol., 2006. **29**(6): p. 665-673.
54. Song, J., et al., *Examination of the oxidation behavior of biodiesel soot.* Combust. Flame, 2006. **146**(4): p. 589-604.
55. Salamanca, M., et al., *Influence of palm oil biodiesel on the chemical and morphological characteristics of particulate matter emitted by a diesel engine.* Atmospheric Environ., 2012. **62**: p. 220-227.
56. Lapuerta, M., et al., *Effect of fuel on the soot nanostructure and consequences on loading and regeneration of diesel particulate filters.* Combust. Flame, 2012. **159**(2): p. 844-853.
57. Bhardwaj, O.P., et al., *Utilization of HVO Fuel Properties in a High Efficiency Combustion System: Part 2: Relationship of Soot Characteristics with its Oxidation Behavior in DPF.* SAE Int. J. Fuels Lubr. , 2014. **7**(3): p. 979-994.
58. Ye, P., et al., *Impact of rail pressure and biodiesel fueling on the particulate morphology and soot nanostructures from a common-rail turbocharged direct injection diesel engine.* IJER, 2014. **17**(2): p. 193-208.
59. Meakin, P., B. Donn, and G.W. Mulholland, *Collisions between Point Masses and Fractal Aggregates.* Langmuir, 1989. **5(2)**: p. 510-518.
60. Park, K., D.B. Kittelson, and P.H. McMurry, *Structural Properties of Diesel Exhaust Particles Measured by Transmission Electron Microscopy (TEM): Relationships to Particle Mass and Mobility.* Aerosol Sci.Technol., 2004. **38**(9): p. 881-889.
61. Fayad, M.A., et al., *Role of Alternative Fuels on Particulate Matter (PM) Characteristics and Influence of the Diesel Oxidation Catalyst.* Environ. Sci. Technol., 2015. **49**(19): p. 11967-73.
62. Vander Wal, R.L. and A.J. Tomasek, *Soot oxidation: dependence upon initial nanostructure.* Combust. Flame, 2003. **134**(1-2): p. 1-9.
63. Wal, R.L.V., *Initial Investigation of Effects of Fuel Oxygenation on Nanostructure of Soot from a Direct-Injection Diesel Engine.* Energy Fuels, 2006. **20**: p. 2364-2369.
64. Strzelec, A., et al., *Nanostructure and burning mode of light-duty diesel particulate with conventional diesel, biodiesel, and intermediate blends.* Int. J. Engine Res., 2017: p. 1-12.
65. Yehliu, K., et al., *Impact of fuel formulation on the nanostructure and reactivity of diesel soot.* Combust. Flame, 2012. **159**(12): p. 3597-3606.
66. Savic, N., et al., *Influence of biodiesel fuel composition on the morphology and microstructure of particles emitted from diesel engines.* Carbon, 2016. **104**: p. 179-189.
67. Ess, M.N., et al., *In situ Raman microspectroscopic analysis of soot samples with different organic carbon content: Structural changes during heating.* Carbon, 2016. **105**: p. 572-585.
68. Seong, H.J., *Impact of oxygen enrichment on soot properties and soot oxidative reactivity.* The Pennsylvania State University, 2010. **PhD Thesis**.
69. Sharma, V., et al., *Structure and chemistry of crankcase and exhaust soot extracted from diesel engines.* Carbon, 2016. **103**: p. 327-338.